Soil Moisture Influence on the Incidence of Summer Mesoscale Convective Systems in the U.S. Great Plains

RACHEL GAAL[a] AND JAMES L. KINTER III[a,b]

[a] George Mason University, Fairfax, Virginia
[b] Center for Ocean–Land–Atmosphere Studies, George Mason University, Fairfax, Virginia

(Manuscript received 11 June 2021, in final form 28 September 2021)

ABSTRACT: Mesoscale convective systems (MCS) are known to develop under ideal conditions of temperature and humidity profiles and large-scale dynamic forcing. Recent work, however, has shown that summer MCS events can occur under weak synoptic forcing or even unfavorable large-scale environments. When baroclinic forcing is weak, convection may be triggered by anomalous conditions at the land surface. This work evaluates land surface conditions for summer MCS events forming in the U.S. Great Plains using an MCS database covering the contiguous United States east of the Rocky Mountains, in boreal summers 2004–16. After isolating MCS cases where synoptic-scale influences are not the main driver of development (i.e., only non-squall-line storms), antecedent soil moisture conditions are evaluated over two domain sizes (1.25° and 5° squares) centered on the mean position of the storm initiation. A negative correlation between soil moisture and MCS initiation is identified for the smaller domain, indicating that MCS events tend to be initiated over patches of anomalously dry soils of ~100-km scale, but not significantly so. For the larger domain, soil moisture heterogeneity, with anomalously dry soils (anomalously wet soils) located southwest (northeast) of the initiation point, is associated with MCS initiation. This finding is similar to previous results in the Sahel and Europe that suggest that induced meso-β circulations from surface heterogeneity can drive convection initiation.

KEYWORDS: North America; Atmosphere-land interaction; Mesoscale systems; Soil moisture

1. Introduction

The largest form of deep convection is the mesoscale convective system (MCS), an organized aggregate of cumulonimbus clouds. This single cloud system has a very large upper cirriform cloud structure and is known for its large size (Houze 2004; Feng et al. 2019). Flash flooding is the prime hazard associated with long-lasting and slow-moving MCSs, but they are also known to produce damaging hail, lightning, and tornadoes (Houze et al. 1990; Houze 2004). Beyond their societal impacts, MCS account for over 50% of the warm season rainfall in the central United States (Fritsch et al. 1986; Ashley et al. 2003; Feng et al. 2016, 2019; Haberlie and Ashley 2019) and up to 75% of extreme rainfall east of the Rocky Mountains in spring and summer (Song et al. 2019). MCS over land therefore contribute greatly to redistributing water and energy over the central United States.

Due to the size of MCS events and the mesoscale circulations that they produce (Houze 2004, 2018), most research on their origins has focused on the large-scale atmospheric environment in which they form. Feng et al. (2019) found that the synoptic-scale environment in which MCS initiation occurs is highly dependent on season and location, with the Great Plains in particular being a hotspot for these events. In the Great Plains specifically, MCS events that occur during the warm season tend to form adjacent to the entrance region of upper-level jets (Peters and Schumacher 2014; Song et al. 2019). With reference to the differences between spring and summer large-scale environments associated with Great Plains MCS, Song et al. (2019) found that frontal systems and an enhanced Great Plains low-level jet were responsible for the development of MCSs in favorable environments, and that the locations of these environments shift northward during the summer.

An important aspect of the Song et al. (2019) findings is that during the summertime, there are two different unfavorable large-scale environments under which MCSs can form. Their results show that the prevailing conditions for both unfavorable conditions include an upper-level ridge within the vicinity of initiation. Under this weak baroclinic forcing, sources of convective triggering could be attributed to small-scale perturbations, including subsynoptic-scale disturbances and influences of the land surface as suggested by Feng et al. (2019). Subsynoptic-scale disturbances responsible for MCS initiations in the Great Plains, such as midtropospheric shortwave perturbations associated with the Rocky Mountains (Wang et al. 2011), occur on shorter time scales and therefore do not provide a sufficient source of predictability for MCS initiation.

How can the land surface influence the formation of MCSs under weak large-scale forcing? Soil moisture and vegetation are known to have an influence on precipitation, because the land surface controls latent and sensible heat flux partitioning (Koster 2004; Miralles et al. 2014; Zhou et al. 2016), which subsequently controls the energy available for convective development and the depth of the planetary boundary layer. Ultimately, in the absence of synoptic-scale forcing, the

Publisher's Note: This article was revised on 17 January 2022 to correct a typographical error in the second-to-last sentence of the abstract.

Corresponding author: Rachel Gaal, rgaal@gmu.edu

DOI: 10.1175/MWR-D-21-0140.1

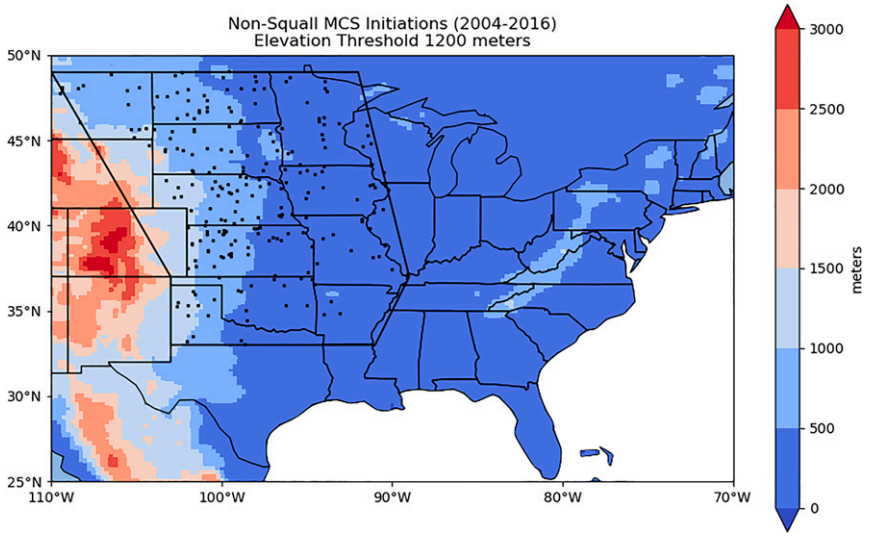

FIG. 1. Region of interest for storm selection that loosely corresponds to the Koster (2004) U.S. hotspot. Exact vertices of boundary are the following: (49°N, 110°W), (37°N, 103°W), (33°N, 103°W), (33°N, 91°W), (37°N, 89°W), (49°N, 92°W). Non-squall-line MCS cases within the region of interest shown geographically. Shading represents elevation in meters.

balance of fluxes will either favor or suppress the triggering of clouds and precipitation.

Research related to soil moisture–precipitation coupling is typically focused on unorganized convection to isolate the signal of the land surface, apart from organized, typically synoptically driven systems like the MCS (e.g., Ford et al. 2015; Guillod et al. 2015). The relationship between the initiation of deep moist convection and soil moisture has been evaluated in different locations with different climatological characteristics, notably in the Sahel (Taylor et al. 2011), a "hotspot" for land–atmosphere interaction according to Koster (2004), all continents (Taylor et al. 2012) and Europe (Taylor 2015). These studies suggest that afternoon rainfall over relatively dry areas is strongest over semiarid regions, and soil moisture heterogeneity on small scales of $O(10)$ km impacts the location of MCS rainfall. This is consistent with a mechanism in which increased sensible heat flux over drier soils and mesoscale variability in soil moisture can drive afternoon deep convection (Froidevaux et al. 2014). Tuttle and Davis (2006) and Trier et al. (2014) discuss the phenomenon of so-called corridor events, wherein MCSs occur over the same region for several consecutive days triggered by soil moisture and atmospheric gradients created by the MCSs themselves.

To examine the role of soil moisture heterogeneity, Baur et al. (2018) modeled the dynamics of convective precipitation development over central Europe. Their convective-permitting simulations showed that differential heating over dry and moist soil patches of different scales generates mesoscale circulations in the planetary boundary layer (PBL). The circulation exhibits divergent motion over anomalously moist patches and convergent motion over anomalously dry patches. The main finding associated with this pattern was that increased convective triggering and precipitation occurs on the downstream side of dry patches. The influence of the soil moisture precipitation coupling decreases with increasing synoptic forcing, and the circulation is most dominant for soil-moisture perturbations at scales between 40 and 80 km.

The Great Plains, as noted by Koster (2004), is a hot spot for land–atmosphere feedback and has been the domain of many smaller case studies focused on soil moisture–precipitation interactions (e.g., Frye and Mote 2010; Ford et al. 2015). Inspired by the conclusions of Song et al. (2019), this work aims to evaluate the favorable land surface conditions for summer MCS initiation in the Great Plains under unfavorable synoptic conditions. It is hypothesized that, when large-scale forcing is weak, MCS initiation can occur in the vicinity of heterogeneous soil moisture conditions, and MCS initiation in the Great Plains is centered in places where conditions are locally drier relative to surroundings consistent with the findings of other studies of semiarid regions. This study will assess the nature of the inhomogeneity of soil moisture at different spatial scales in order to further elaborate the possible mechanism. In section 2, the main data sources are presented and in section 3, the main methodology is described. Section 4 presents the results identifying favorable land surface conditions and other atmospheric conditions with respect to MCS initiation. A discussion and summary are provided in section 5.

2. Data sources

To establish a relationship between soil moisture and MCS development, cases of MCSs and soil moisture observations in the Great Plains during boreal summer are both needed for analysis. For this study, three datasets are used, one of which is an observational catalog of convective events that has not been used previously for this purpose. This combination of datasets in the Great Plains applied to the above hypothesis is

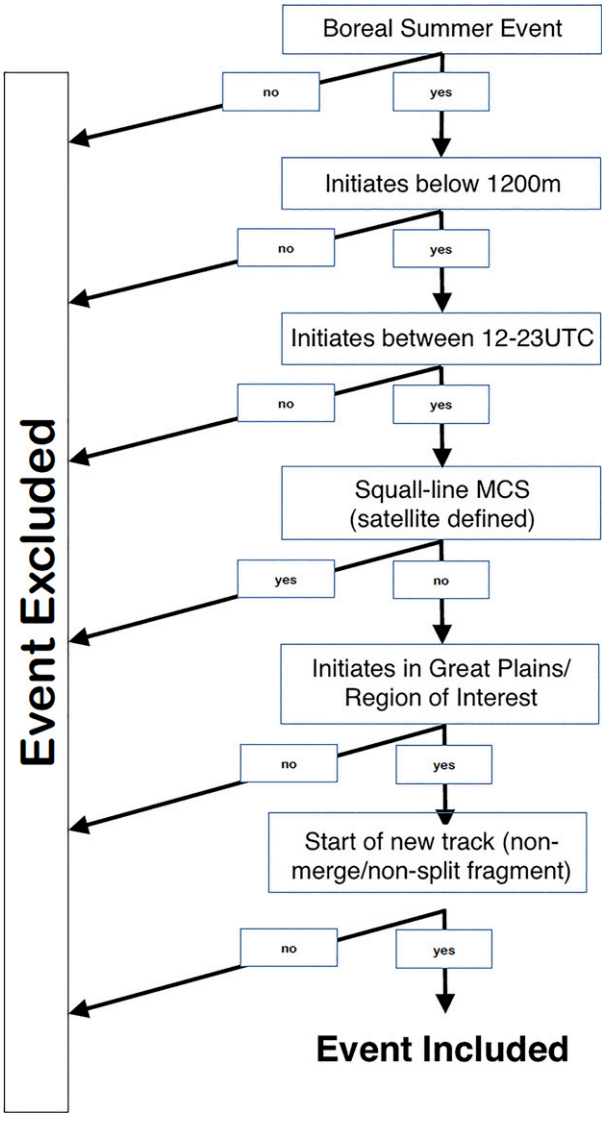

FIG. 2. Decision tree detailing the choices made to include or exclude MCS cases. This figure is adapted from Fig. 1 in Ford et al. (2015). Initiation height is determined by elevation of initiation mean latitude and longitude point. Squall-line MCS refers to the classification of the storm track in MCS2019.

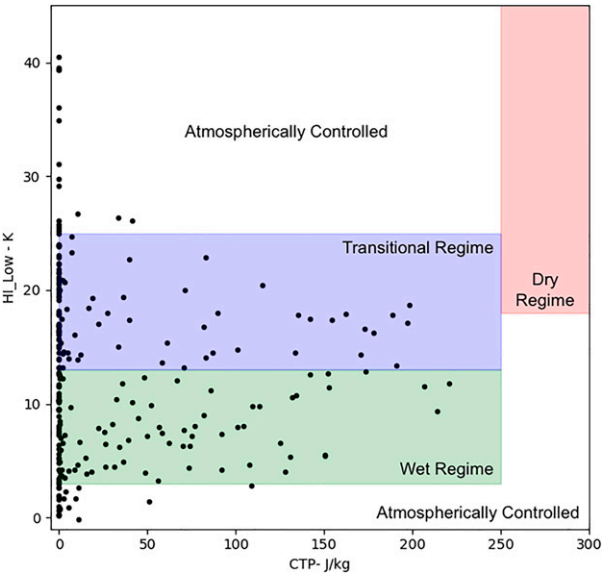

FIG. 3. Convective triggering potential (CTP) and low-level humidity index (HI_Low) diagram, where each case can fall into one of four categories: dry coupling, wet coupling, transitional, or atmospherically controlled. These threshold values are augmented from the original values outlined in Findel and Eltahir (2003a,b), based on others who have found the original distributions to vary geographically and depend on the source of the data.

unique to this study. Each dataset is described below in a respective subsection.

a. MCS event database

MCS events in this study are taken from the MCS database (Feng et al. 2019; doi.org/10.5439/1571643; Version 1 released December 2019) covering the contiguous United States east of the Rocky Mountains, for 2004–16 (hereafter MCS2019). To produce MCS2019, an updated version of the flexible object tracker (FLEXTRKR) algorithm (Feng et al. 2018) was applied to NASA Global MergedIR satellite infrared brightness temperature (Tb) data (Janowiak et al. 2001) and the GridRad mosaic 3D Next-Generation Radar (NEXRAD) dataset (Bowman and Homeyer 2017). The method tracks significantly sized cold cloud shields (CCS; Tb < 241 K) that are generated by deep convection, and then uses radar to define the convective and precipitation features. MCS2019 is at an hourly resolution and a 4 km $\times$ 4 km spatial resolution.

Within MCS2019, each tracked storm is defined as a large CCS (area $> 6 \times 10^4$ km^2) containing a precipitation feature (PF) with a major axis length > 100 km that persists for at least 6 h and a convective feature containing radar reflectivity > 45 dBZ at any vertical level (Feng et al. 2019). Earlier work suggests that achieving mesoscale circulation in the midlatitudes requires an MCS to have a length scale of 100 km and duration of at least 3 h (Parker and Johnson 2000). The MCS events tracked in Feng et al. (2018, 2019) are longer-lived MCSs (i.e., events with PFs persisting for at least 6 h).

For each of these tracked storms, MCS2019 provides standard statistical information, such as location, and derived information about the MCS lifetimes (i.e., developing, mature, decaying), as indicated by the rate of growth and the scale of PFs within the MCS. In this study, only the convection initiation (CI) stage of an MCS (defined as the "first hour when a CCS is detected") is used, which is represented by the first timestamp of a new storm track. The use of CCS, rather than precipitation, to define CI has to do with the timing of the partitioning of sensible and latent heat flux, along with the different mechanisms involved in the soil moisture–precipitation feedback process; these typically occur before substantial precipitation is generated. It has been suggested (e.g., Ford et al. 2018) that the timing and location of where precipitation begins does not always accurately represent when and where CI (as defined by Feng et al. 2019) occurs, therefore investigating soil

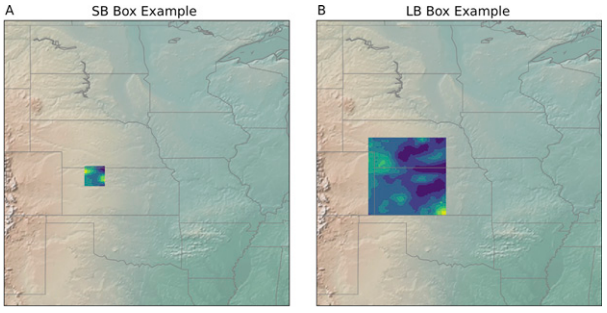

FIG. 4. Examples of (a) small box (SB) area (1.25° × 1.25° box) centered around a latitude and longitude coordinate and (b) large box (LB) area (5° × 5° box) centered around a mean latitude and longitude coordinate.

moisture conditions associated with convection initiation is more appropriate than using precipitation as a marker for CI. Other information from MCS2019 used in this study includes the location of MCSs classified by regions outlined in Feng et al. (2019), and information about MCS type (non-line versus squall line) based on radar-defined features of MCS structure, such as major axis length and eccentricity.

b. Land surface data

Soil moisture data (layer 1: 0–7 cm, layer 2: 7–28 cm) and 2-m temperature data matching the same period are taken from the European Centre for Medium-Range Weather Forecasts (ECMWF) ERA5-Land reanalysis (Muñoz Sabater 2019; released July 2019). This high-resolution (0.1° × 0.1°) hourly dataset, produced by replaying the land component (Orbe et al. 2017) of the ECMWF ERA5 climate reanalysis (Hersbach et al. 2018, 2020), which is available from 1981 to the present, was used in order to have an accurate representation of the smaller scale terrestrial details (Balsamo et al. 2015). First-order conservative remapping is used to match the ERA5-Land data to the MCS database resolution.

c. Atmospheric data

The ECMWF ERA5 reanalysis (available from 1979 to the present; Hersbach et al. 2020) is employed for all atmospheric variables used in this study, including total precipitation, horizontal and vertical velocities, and boundary layer height, and is used to calculate other local instability parameters such as CAPE and divergence. First-order conservative remapping is used on all ERA5 variables to match the MCS database resolution.

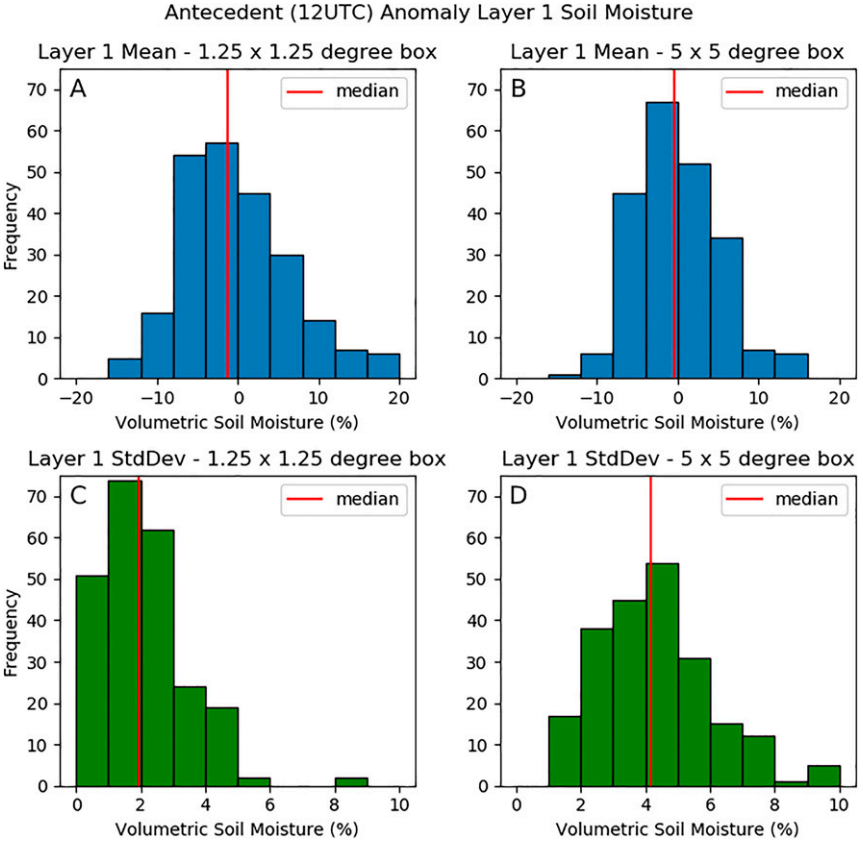

FIG. 5. Histograms of antecedent (1200 UTC) layer 1 volumetric soil moisture anomaly mean and standard deviation values with respect to number of initiations. (a) Counts of mean soil moisture values in SB area, (b) counts of mean soil moisture values in LB area, (c) counts of soil moisture standard deviation values in SB area, and (d) counts of soil moisture standard deviation values in LB area.

3. Methodology

a. MCS case criteria

Based on these datasets, the period of analysis covers boreal summer (June–August), 2004–16. Information from MCS2019 is used to isolate boreal summer cases of MCSs where (i) the track is a non-split/nonmerged storm (i.e., the first time step of each tracked storm is an initiation and not a fragment of an already mature MCS), and (ii) synoptic-scale influences are not the main driver of the development of these storms (i.e., including only "non-line" classified storms). Using daytime-only storms (1200–2300 UTC) to isolate the influence of the land surface on CI is another key choice in partitioning cases. A detailed region of interest for storm selection is identified in Fig. 1, which is based on the northern Great Plains (NGP) and southern Great Plains (SGP) sectors of analysis in Feng et al. (2019), and augmented to better fit the Great Plains region by only including areas between 33°–49°N and 91°–110°W, and below 1200 m in elevation. The latter criterion removes cases where orographic lifting is aiding in the initiation of convection, namely, in the foothills of the Rockies. A total of 240 cases meet these criteria, which are geographically shown in Fig. 1 with reference to their elevation. A decision tree illustrating the selection algorithm for MCS cases is in Fig. 2.

To verify the assumption that the chosen cases are not atmospherically controlled (or not occurring in a synoptically favorable environment), the convective triggering potential (CTP) and low-level humidity index (HI_Low) (Findell and Eltahir 2003a,b) are calculated for each case. CTP–HI_Low is a straightforward way to characterize if and how early morning atmospheric profiles of humidity and temperatures influence the development of the boundary layer through the daylight hours. It is ultimately focused on the different effects of boundary layer deepening versus moistening in allowing the planetary boundary layer (PBL) to reach the level of free convection for convective triggering to occur. This makes it suitable for determining whether or not daytime rainfall, if any, is synoptically controlled. Findell and Eltahir (2003a,b) characterize "wet coupling" as a regime where convection and cloud formation is preferred over moist soils, "dry coupling" favors clouds over dry soils, "atmospherically controlled" areas are insensitive to land surface states, and "transition" regimes are subtle and complicated by other factors beyond those measured by CTP and HI_Low. They initially proposed ranges for coupling regimes that suggest when and how convective clouds and precipitation are likely to be triggered depending on atmospheric and surface conditions. Subsequent studies by others have found that distributions may deviate from the ranges of CTP and HI_Low they proposed, can vary geographically, and depend on the source of the data (i.e., Ferguson and Wood 2011; Roundy et al. 2014; Roundy and Santanello 2017). However, some general characteristics have emerged:

- Wet coupling tends to be prevalent at values of HI_Low between about 3 and 13 K, CTP values up to 250 J kg^{-1}, and even sometimes for negative values of CTP.
- Dry coupling is likely for cases with both CTP above 250 J kg^{-1} and HI_Low above 18 K.

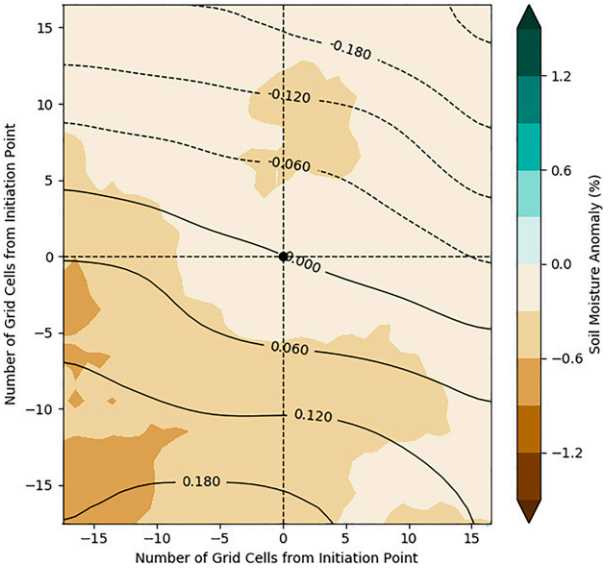

FIG. 6. 1200 UTC soil moisture anomaly (%; shading) and T2m anomaly (K; contouring) average composite for SB area centered around the mean initiation point (center dot). For clarity, the spatial mean T2m anomaly was removed from each event. Significant soil moisture and T2m anomalies are to be stippled at the 95% level. The labeled number of grid cells is representative of the 4-km grid spacing used in the MCS database.

- Positive values of CTP up to 250 J kg^{-1} with HI_Low between 13 and 25 K that are not in the dry coupling regime are mostly in a transitional regime.
- Other values are in the atmospherically controlled regime.

A CTP–HI_Low chart for the 240 cases selected by the algorithm illustrated in Fig. 2 is shown in Fig. 3, which is labeled to show which cases are dry coupling, wet coupling, transitional, and atmospherically controlled based on the CTP and HI_Low distributions described above. The majority of cases in Fig. 3 are in the transitional regime (where either moistening or deepening of the PBL from surface fluxes would be responsible for convective triggering; 95 cases), and the wet-coupled regime (where exclusively boundary layer moistening from surface fluxes would be responsible for convective triggering; 108 cases), with only 37 cases that could be classified as atmospherically controlled out of 240. While these ranges of CTP and HI_Low are only indicative and not prescriptive, this classification supports the identification of the 240 MCS initiation cases that are more likely to be influenced by the land surface state. For comparison, all boreal summer radar-classified squall cases that occur in the region of interest during daytime hours (109 cases; summer squalls) are also analyzed.

b. Study area

Using the first mean latitude and longitude point of a selected MCS track as the center, representative of the storm initiation, two domains with different sizes are demarcated for each event: one smaller box (1.25° × 1.25° box; hereafter "SB"), and a larger box (5° × 5° box; hereafter "LB"), both aligned with constant latitude and longitude. Examples of these two boxes for an

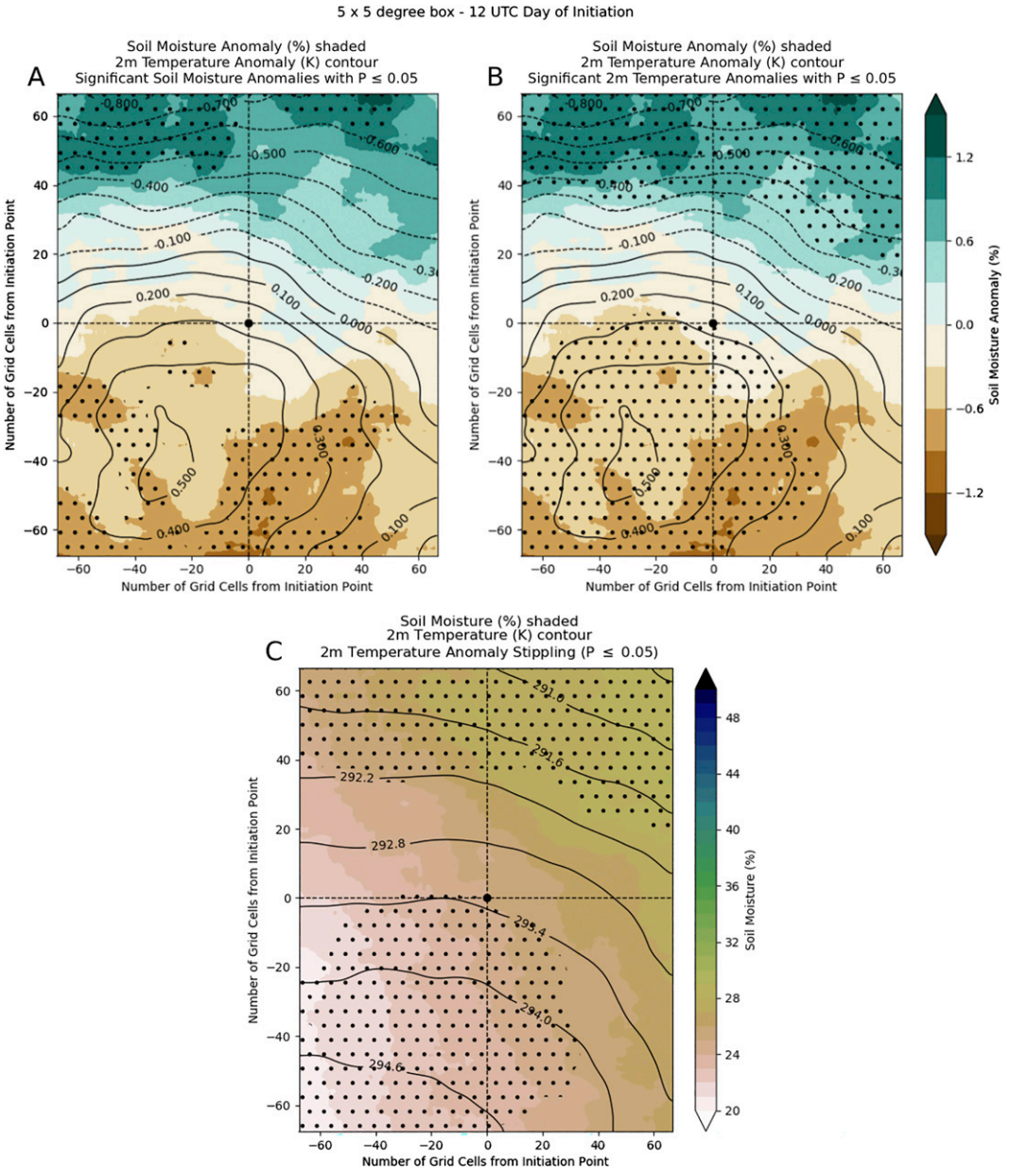

FIG. 7. (a) 1200 UTC soil moisture anomaly (%; shading) and (b) T2m anomaly (K; contouring) average composite for LB area centered around the mean initiation point (center dot) with (a) significant soil moisture anomalies stippled at the 95% level or (b) significant T2m anomalies stippled at the 95% level. For clarity, the spatial mean T2m anomaly was removed from each event. (c) Full-field soil moisture (%; shading) and T2m (K; contouring) with T2m stippling from Fig. 7b. The labeled number of grid cells is representative of the 4-km grid spacing used in the MCS database.

arbitrary mean latitude–longitude point are shown in Fig. 4. The SB (Fig. 4a) is used to identify the presence of soil moisture heterogeneity at the tens of kilometer scale surrounding the immediate area of initiation, as in Taylor et al. (2011). The LB (Fig. 4b) was chosen to detect the effect of the large-scale zonal SM gradient that exists in the Great Plains (dry to moist transitional region) associated with land–atmosphere interaction zones previously identified as "hot spots" (Koster 2004).

Analyses of Great Plains MCS initiations using standard methods (e.g., Taylor et al. 2011), superposed epoch (Adams et al. 2003) and atmospheric column time series analyses, are carried out using the two different sized boxes, aiming to answer the following questions:

1) What is the average anomaly soil moisture (SM) and 2-m temperature (T2m) antecedent to initiation?

2) What is the spatial structure of soil moisture and land surface temperature anomalies, and how do they evolve prior to CI?
3) How does the local atmospheric environment evolve prior to initiation?

In particular, the evolution of land surface variables and the local atmospheric environment prior and subsequent to MCS initiations has not previously been examined. SM and T2m anomalies are calculated by subtracting the mean monthly diurnal cycle. Full fields are only used when evaluating the evolution of the local atmospheric environment. It should be noted that ERA5 has deficiencies in its representation of the diurnal cycle of precipitation, particularly in cases of organized deep convection. Nevertheless, we consider the quality of ERA5 to be adequate for the analysis herein.

c. *Evaluation of significance*

Confidence intervals to assess the significance of the relationship between land surface variables and MCS initiations were calculated by using a permutation technique within a bootstrapping resampling method. This procedure accounts for the fact that the SM and T2m anomaly fields used in all cases, which are non-Gaussian in nature, are not only spatially correlated but temporally correlated as well. SB and LB composites of all cases were created at the same locations, times and dates (i.e., latitude, longitude, month, day, and 1200 UTC is preserved), but with soil moisture taken from a different year, to create a synthetic case set. For example, the SB and LB case composites from 2004 can be created using 2011 soil moisture anomaly fields (and 2005 case composites can be created using 2014 soil moisture anomaly fields, etc.). This permutation is done for all years, wherein the years are randomized without replacement and without matching years. The individual case composites are then made as usual, and averaged to create a mean MCS event composite. This entire procedure is repeated 1000 times to ultimately produce 1000 unique mean MCS event composites. At each grid point, the 1000 unique values are ranked to create a distribution, and two-tailed quantiles are calculated for that distribution. The grid point is deemed significant if the original mean MCS event soil moisture value exceeds either specified quantile value. The significance testing for the T2m is analogous. Any significance testing for the summer squall subset follows the same protocol as described here, except for using the corresponding case dates and locations for the summer squall events.

4. Results

To answer the first question, histograms are generated of the spatial mean and standard deviation soil moisture values antecedent to the storm initiation at 1200 UTC for SB and LB areas. The antecedent time is used rather than the exact hour/beginning timestamp of each track in order to remove the possibility that rainfall generated by the MCS itself affects the detection of the CCS, to minimize the error possibly introduced by biases in the representation of convection in ERA5, and because the influence of the land surface on the development of convection is highly dependent on the early morning condition of the atmosphere (Findell and Eltahir 2003a). For the SB area (Fig. 5a), the mean soil moisture (layer 1—upper 7 cm) in the majority of cases is dry, but not significantly so. There is also a long upper tail in the distribution of Fig. 5a indicating that some cases have significantly anomalously wet conditions. Figure 5c shows an abundance of smaller standard deviation values, implying that the conditions within the SB area are largely homogeneous. The standard deviation values in the LB area (Fig. 5d) are higher compared to those calculated from the SB area (Fig. 5c), suggesting more heterogeneous conditions that exist within the domain.

While these characterizations are valuable, the histograms do not provide any information about the spatial structure of soil moisture that exists antecedent to initiation and whether or not the heterogeneity implied to exist in the LB areas is organized in any way. To understand this, all SB and LB SM and T2m anomalies are averaged, respectively, to produce

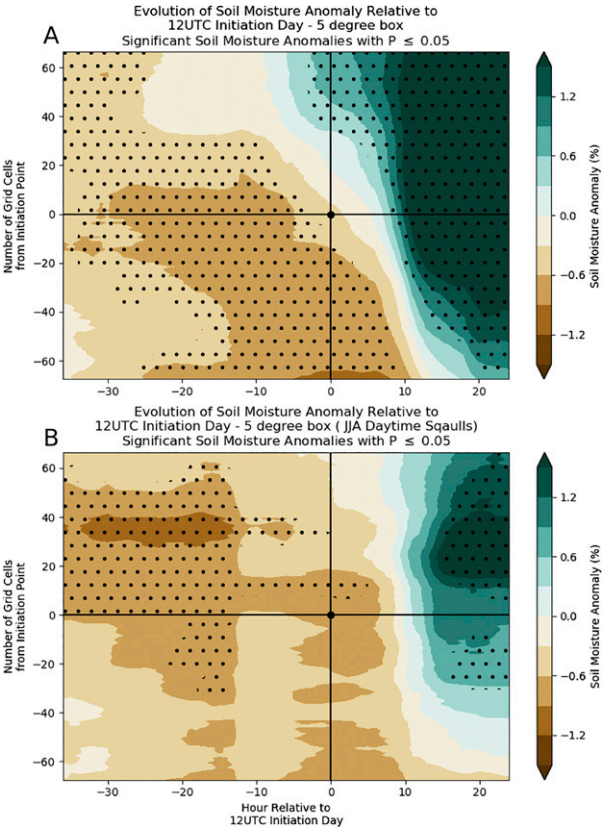

FIG. 8. Zonally averaged 5° mean MCS soil moisture (%) event composites plotted through time, from 36 h prior to 1200 UTC to 24 h after 1200 UTC, as a function of north–south distance from the mean point of initiation, for (a) non-squall-line cases and (b) squall-line cases. Significant soil moisture anomalies are stippled at the 95% level.

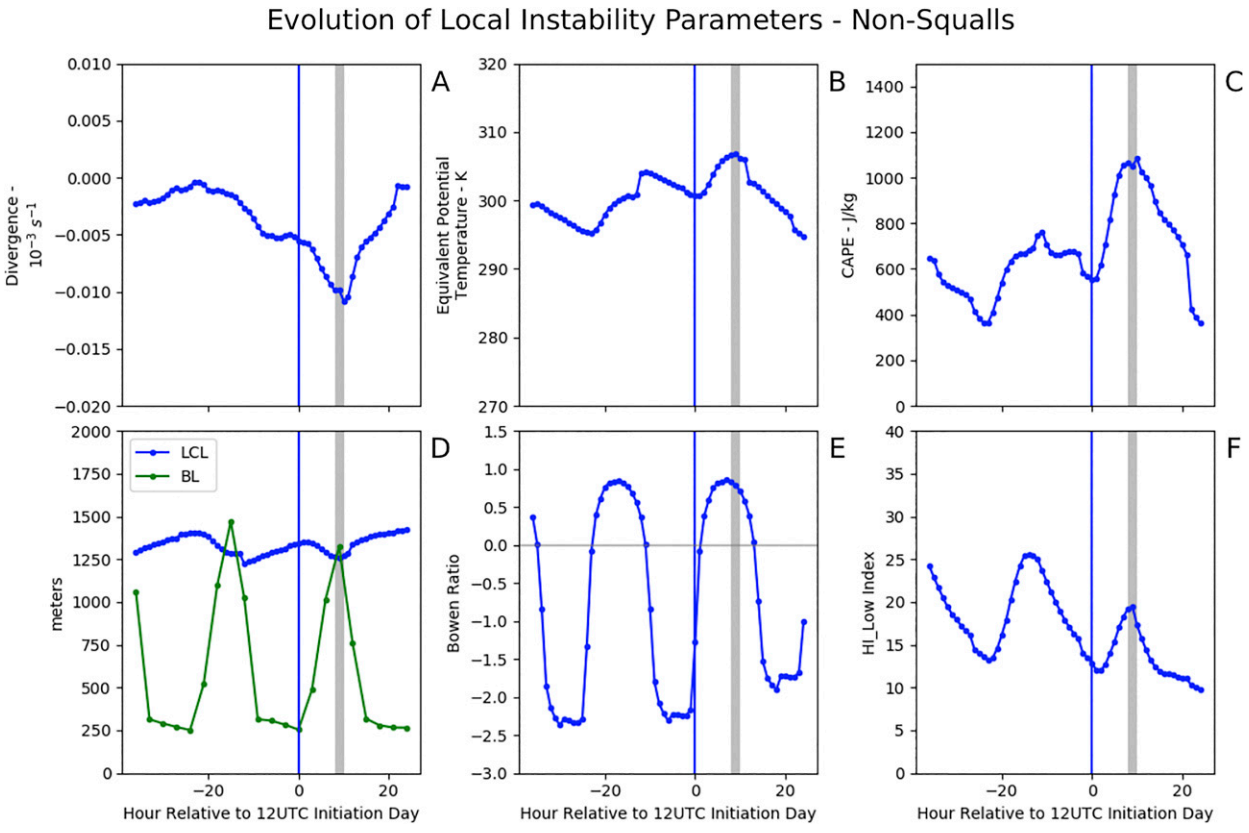

FIG. 9. Evolution of local instability parameters for non-squall-line events: (a) divergence (10^{-3} s^{-1}), (b) equivalent potential temperature (K), (c) convective available potential energy (J kg^{-1}), (d) lifted condensation level (m) and boundary layer height (m), (e) Bowen ratio (dimensionless), and (f) HI_Low index. The gray band is located between 8 and 10 h after 1200 UTC and is representative of the timeframe of the majority of initiations.

composites of these anomaly fields. Figure 6 shows the composite soil moisture (shaded) and T2m (contoured) anomaly fields for the SB area surrounding the mean point of initiation at 1200 UTC. We evaluated the significance of the soil moisture and T2m values in this composite, and no values were significant at the 95% level. This composite supports the conclusion drawn from the soil moisture histogram (Fig. 5a), wherein the SB area is skewed near normal and near-dry, but not significantly so.

In Fig. 7, the analogous composite for LB areas is shown. The shading and line contours are the same in both Figs. 7a and 7b. Soil moisture and temperature anomaly gradients are apparent, with anomalously dry soils (anomalously hotter temperatures) in the southwest quadrant and anomalously wetter soils (anomalously cooler temperatures) in the northeast quadrant. The mean point of initiation is over anomalously drier soils (following from Fig. 6), but examining a larger area surrounding the point of initiation reveals that this point lies within a transitional region. The significance shading differs from each plot, where Fig. 7a has stippling for significant soil moisture anomaly values at the 95% level, and Fig. 7b has stippling for significant T2m anomaly values at the 95% level.

As depicted in Fig. 7, the event anomalies are different from zero, with a confidence of 95%, indicating that this emerging pattern is different from climatology. It is also apparent that the SM state is an appropriate proxy for T2m, with a large anticorrelation (spatial correlation = −0.93). This is consistent with the possibility that, in the area of initiation, convection could be induced by mesoscale circulations caused by the temperature gradient and related pressure gradient that arises in the vicinity of the SM gradient (Taylor et al. 2011; Taylor 2015; Baur et al. 2018). Since the atmosphere is likely to respond to absolute gradients, we evaluated the full-field SM and T2m where MCSs occurred, depicted in Fig. 7c. This figure is a hybrid of the significance shading in Fig. 7b and the mean full-field SM and T2m that is present in those locations where the MCS initiation occurred. The figure shows that the anomalous SM and T2m gradients reinforce a mean background southwest–northeast-oriented gradient of the same variables, and that this absolute gradient is substantially larger (~7% per ~5 K range over the 5° boxes) compared to the anomalous gradient (~2% per ~1 K range). While Fig. 7 provides valuable information, it is still unclear, how these gradients evolve prior to MCS initiation because this is only a snapshot of the soil moisture and temperature at 1200 UTC on initiation day.

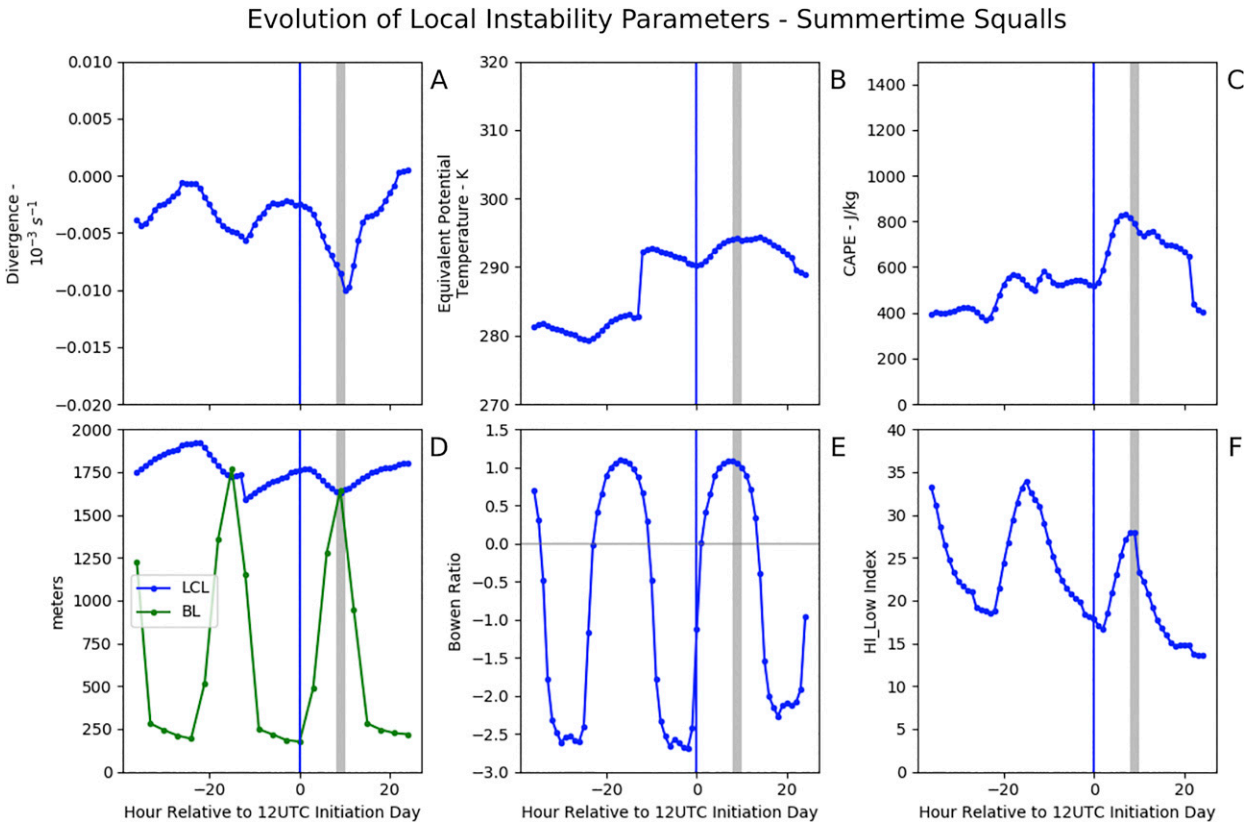

FIG. 10. Evolution of local instability parameters for summertime squall events: (a) divergence (10^{-3} s^{-1}), (b) equivalent potential temperature (K), (c) convective available potential energy (J kg^{-1}), (d) lifted condensation level (m) and boundary layer height (m), (e) Bowen ratio (dimensionless), and (f) HI_Low index. The gray band is located between 8 and 10 h after 1200 UTC and is representative of the timeframe of the majority of initiations.

To get a better idea of the evolution of the soil moisture state prior to initiation, zonally averaged 5° mean MCS event composites are plotted through time (hourly) from 36 h prior to 1200 UTC on initiation day to 24 h after 1200 UTC on initiation day, as shown in Fig. 8a. The entire domain is anomalously dry prior to 1200 UTC, with moistening of the northernmost portion of the domain occurring <10 h before 1200 UTC. This moistening primes the soil moisture to acquire the gradient depicted in Fig. 7. It then takes ~10 h for the MCS event rainfall to completely moisten the domain, with about half of initiations (~120) occurring between 2000 and 2200 UTC. This potential precursor of initiation—the gradual surface moistening a few hundred kilometers to the north—could be important because of the dynamical and thermodynamic processes that are generated in response to a surface moisture gradient. To check whether or not squall-like storms have the same soil moisture profile through time, the same analysis was performed for the group of summer squalls (109 cases) and is depicted in Fig. 8b. The entire domain is anomalously dry with no addition of moisture in the domain, except after the onset of event-related precipitation >10 h after 1200 UTC.

Another important component in understanding how soil moisture influences the initiation of MCS events is to explore the local atmospheric environment, and in particular, instability parameters. A selection of local instability parameters is plotted in Fig. 9. These variables were calculated through time at hourly intervals (with the exception of boundary layer height, which is calculated at 3-h intervals) by taking the spatial average over the LB domain for each case (taking the spatial average over the SB domain was also done but did not change the results). The average of the distribution of values is plotted.

The majority of the parameters in question behave in a manner expected for convective activity; around the time of initiation, there is increased convergence, CAPE, equivalent potential temperature, and a decrease in LCL with an increase in the boundary layer height, although relatively shallow. Higher values of convergence are found to occur <10 h before 1200 UTC, coinciding with the moistening in the northernmost part of the LB (viz. Fig. 8a). The Bowen ratio, depicted in Fig. 9e, stays below 1 during the day, indicating a dominant latent heat flux and moistening of the boundary layer/lowering of the LCL during daytime hours. This is also supported by the HI_Low index in Fig. 9f, which indicates sufficient moisture is present in the vicinity of the initiation. The same analyses done for the summertime squall cases show an apparent dominant sensible heat flux at the surface (Fig. 10), with lower equivalent potential temperature,

higher LCL/BL heights, a Bowen ratio above 1, but a HI_Low profile that progresses into HI_Low values typically associated with atmospherically controlled regions.

One of the main influences on CI is the wind field and associated horizontal wind shear. In particular, within the LB area, the direction of the wind is important in generating vertical motion, ultimately playing a role in induced mesoscale circulations that have been found to influence MCS initiations in other regions. Using pressure-level ERA5 data, full wind fields at three levels are shown for the LB areas in Figs. 11a–c. The wind vectors have the same units and scaling for all plots. Near the surface (900 hPa; Fig. 11a), winds are southwesterly, flowing from anomalously drier areas into the transitional region, and converging over anomalously wetter areas where the wind speed is reduced. At 700 hPa (Fig. 11b), a veering of the wind field occurs throughout the domain, with varying degrees of south-southwesterly winds. At 500 hPa (Fig. 11c), the steering winds are in the same south-southwesterly direction and at higher speeds.

The background wind pattern consists of convergence downstream and divergence upstream of the drier portions of the domain. To explore whether or not an updraft is associated with low-level convergence, the evolution of vertical velocity is also examined, which is depicted in Fig. 12. It is apparent that at 1200 UTC (in particular at 700 hPa) there is an increased amount of convergence over the mean point of initiation, which further intensifies until the initiation in the later afternoon. The convergence maximum is centered just south of the mean initiation point, coinciding with the drier soil moisture portions of the area (viz. Fig. 7). A comparison of the vertical velocity evolution for squall-line cases is shown in Fig. 13.

5. Discussion and conclusions

This study aims to understand how summer MCSs can form in the Great Plains under unfavorable synoptic conditions with specific consideration of land surface conditions. While this question has been addressed in other locations, notably the semiarid, subtropical Sahel (Taylor et al. 2011) and the relatively moist northwestern region of Europe (Taylor 2015; Baur et al. 2018), in this study, an MCS event catalog—MCS2019 (Feng et al. 2019)—is used to evaluate MCS initiations in the Great Plains. By isolating MCS cases where synoptic-scale influences are not the main driver of development (i.e., evaluating only non-squall-line storms), the antecedent soil moisture conditions (1200 UTC) are evaluated over domains of different sizes (1.25° and 5°), centered on the mean position of the storm initiation, in order to evaluate the scale-dependent characteristics of MCS initiation. At the smaller scale, conditions are fairly homogeneous, with some events having dry SM and other events having wet SM. The ratio of dry to wet cases in the smaller domain is about 1.3–1.4, i.e., there are 30%–40% more dry cases than wet; however, the majority of cases are not significantly drier. At the larger scale, there is more soil moisture heterogeneity, with anomalously dry soils (anomalously wet soils) located

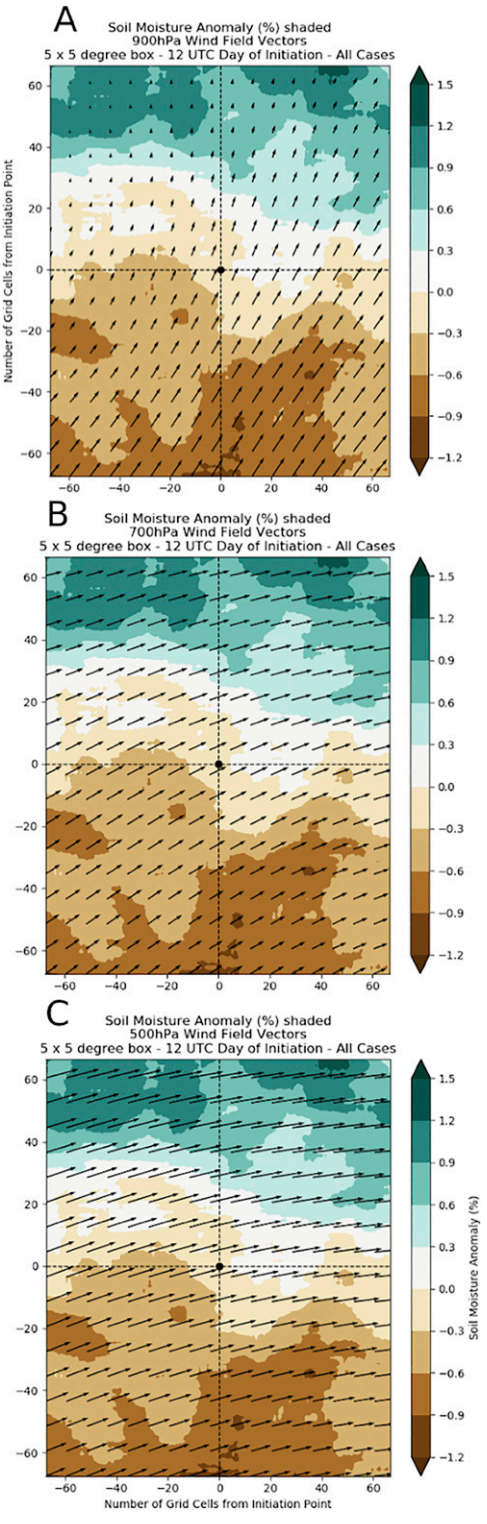

Fig. 11. Wind field vectors at (a) 900, (b) 700, and (c) 500 hPa, with soil moisture anomaly (%; shading) average composite for LB centered around the mean initiation point (center dot). The labeled number of grid cells is representative of the 4-km grid spacing used in the MCS database.

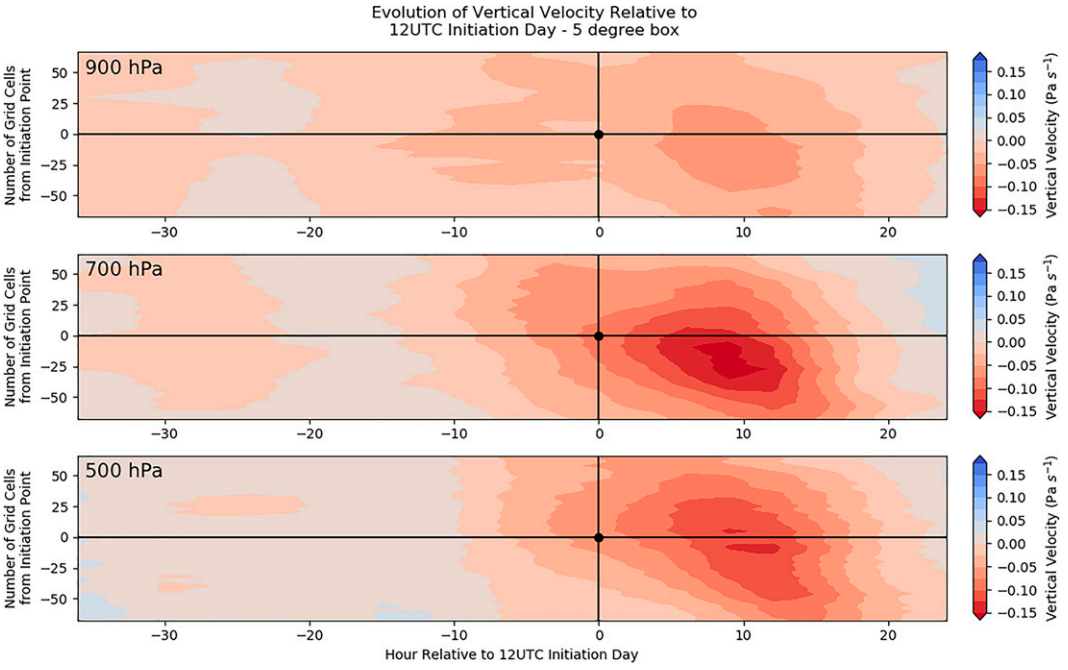

FIG. 12. Zonally averaged 5° mean MCS vertical velocity (Pa s^{-1}) non-squall-line event composites plotted through time, from 36 h prior to 1200 UTC to 24 h after 1200 UTC, as a function of north–south distance from the mean point of initiation.

southwest (northeast) of the initiation point, and a distinct soil moisture gradient that coincides with a temperature gradient at the surface. This gradient evolves from a more homogeneous anomalously dry domain by a gradual moistening of the area ~100–300 km north of the initiation point <10 h before 1200 UTC.

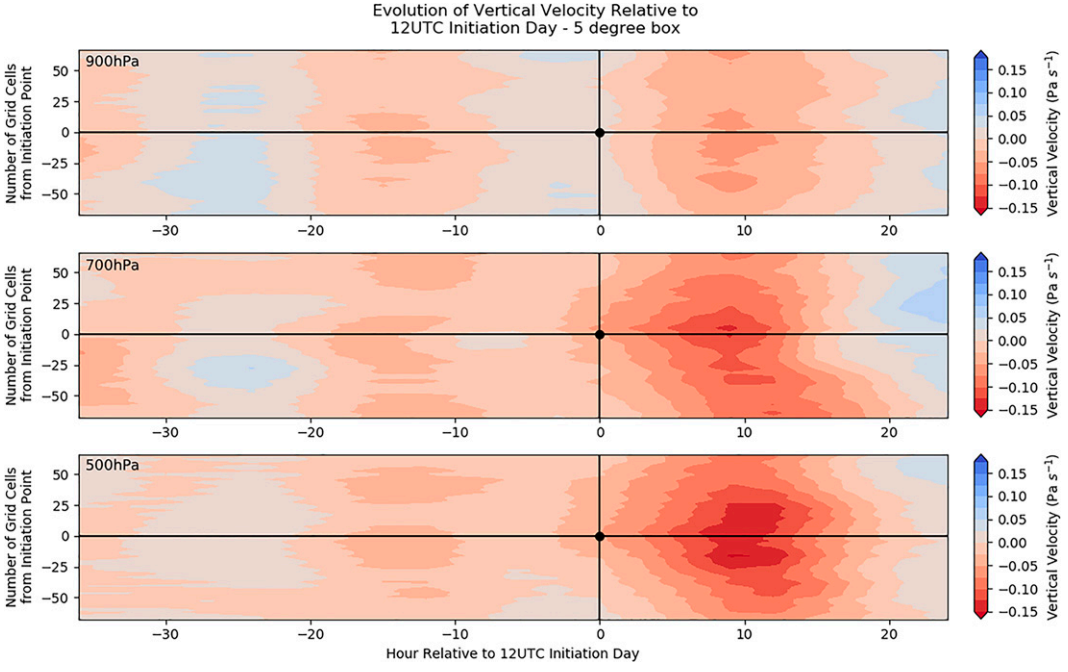

FIG. 13. Zonally averaged 5° mean MCS vertical velocity (Pa s^{-1}) summertime squall event composites plotted through time, from 36 h prior to 1200 UTC to 24 h after 1200 UTC, as a function of north–south distance from the mean point of initiation.

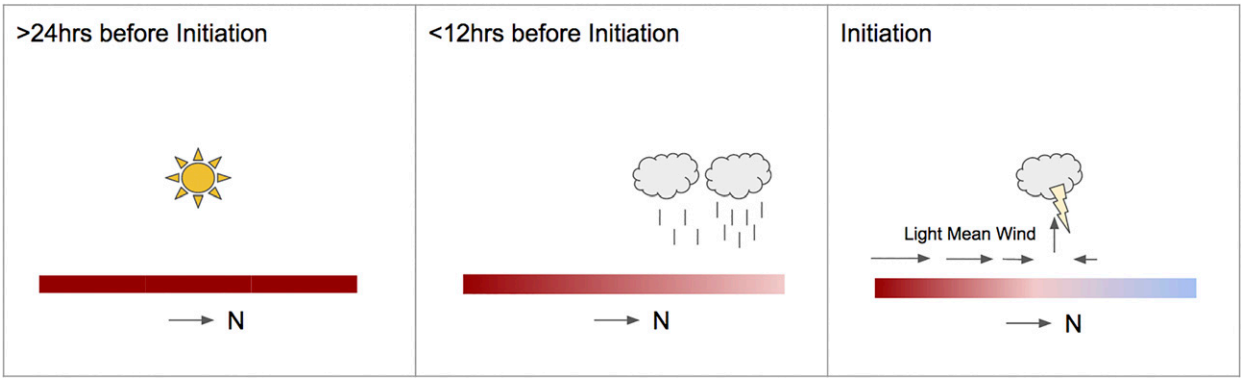

FIG. 14. Schematic depicting the impact of soil-moisture heterogeneity on convective initiation. In the last panel, light synoptic winds create an ascent region (upward arrow) where the shallow area of low-speed winds oriented over moist soils opposes the mean wind. The preferred location for convective initiation in this study coincides with the ascent region induced by the heating gradient at the downwind edge of the dry patch.

A pressure gradient near the surface develops with the temperature gradient, which increases the low-level southwesterly wind. The southwesterly wind at the surface advects warm air from over anomalously hot/dry soils toward the anomalously wet soils, causing two distinct air masses to meet. This induces upward motion in the transition zone between anomalously dry and wet soils. In addition, the direction of the background wind sets up an area of convergence (divergence) over anomalously wet (dry) soils, intensifying the updraft region at the downstream side of dry anomalies within the transitional region. The convergence due to diminishing low-level winds and veering of the wind with height further amplifies the upward motion in this area and eventually results in the formation of an MCS later in the day.

A schematic of this process is illustrated in Fig. 14. Because the large-scale atmospheric forcing is weak, and secondary processes are needed in order to initiate an MCS, the important part of this process is the moistening to the north of the initiation point, which sets up a soil moisture and temperature gradient and influences the dynamic and thermodynamic processes in the atmosphere. Although it has not been shown that the moistening to the north is a necessary condition for MCS initiation in weak synoptic environments, it is reasonable to assume that, without the gradient present, other large-scale lifting mechanisms would be necessary, which are mainly coincident with synoptic-scale weather features that are not present in the cases considered here.

TABLE 1. A comparison table of studies and the corresponding scales at which soil moisture heterogeneity was found to be most influential.

Scientific study	Area of study	Most influential scale of heterogeneity
Baur et al. (2018)	Central Europe	40–80 km
Taylor et al. (2011)	Sahel	$O(10)$ km
Taylor et al. (2012)	Global	$O(50)$ km
Taylor (2015)	Europe	10–40 km

The presence of this soil heterogeneity as a potential trigger of MCS initiation in the Great Plains is similar to previous results in the Sahel and Europe (Taylor et al. 2011; Taylor 2015) that suggest the meso-β circulations induced by soil heterogeneity are prime drivers of MCS initiation. However, those studies were carried out in different geographical areas, with very different climatologies, and they did not account for the synoptic environment when partitioning MCS initiations. The scale at which the heterogeneity was found to be most influential in the aforementioned studies was also smaller (Table 1) compared to the scale of heterogeneity in this particular study [$O(100)$ km]. There are a number of factors that could influence the differences in results, namely, the difference in study location and the sample size (240 in this study versus >2000 cases in Taylor et al. (2011), Taylor (2015)).

While a goal of this work is to understand how soil moisture influences the location of MCS initiations, it is important to note that identifying the mechanisms associated with soil moisture and its influence on MCS initiations is beyond the scope of this study and requires a more in-depth analysis using convective-permitting modeling, such as the experiments performed in Baur et al. (2018). The results in this paper are also based on one land surface reanalysis dataset (ERA-5 Land); the need to perform the same analyses using multiple SM and T2m datasets is emphasized by Ford et al. (2018).

Acknowledgments The authors thank Paul Dirmeyer, Cristiana Stan, and Kathleen Pegion for helpful comments on the study, Zhe Feng for providing the MCS data and documentation, and both reviewers for their helpful comments concerning our analyses. The first author was supported by a Provost's Fellowship from George Mason University. The second author was supported by grants from the National Science Foundation (1338427), the National Oceanic and Atmospheric Administration (NA14OAR4310160), and the National Aeronautics and Space Administration (NNX14AM19G).

Data availability statement ERA-5 and ERA-5 land data analyses are generated using Copernicus Climate Change Service information (2004–16); neither the European Commission nor ECMWF is responsible for any use that may be made of the Copernicus information or data it contains. MCS events in this study are openly available at https://doi.org/10.5439/1571643 as cited in Feng et al. (2019).

REFERENCES

Adams, J. B., M. E. Mann, and C. M. Ammann, 2003: Proxy evidence for an El Niño-like response to volcanic forcing. *Nature*, **426**, 274–278, https://doi.org/10.1038/nature02101.

Ashley, W. S., T. L. Mote, P. G. Dixon, S. L. Trotter, E. J. Powell, J. D. Durkee, and A. J. Grundstein, 2003: Distribution of mesoscale convective complex rainfall in the United States. *Mon. Wea. Rev.*, **131**, 3003–3017, https://doi.org/10.1175/1520-0493(2003)131<3003:DOMCCR>2.0.CO;2.

Balsamo, G., and Coauthors, 2015: ERA-Interim/land: A global land surface reanalysis data set. *Hydrol. Earth Syst. Sci.*, **19**, 389–407, https://doi.org/10.5194/hess-19-389-2015.

Baur, F., C. Keil, and G. C. Craig, 2018: Soil moisture–precipitation coupling over Central Europe: Interactions between surface anomalies at different scales and the dynamical implication. *Quart. J. Roy. Meteor. Soc.*, **144**, 2863–2875, https://doi.org/10.1002/qj.3415.

Bowman, K. P., and C. R. Homeyer, 2017: GridRad—Three-dimensional gridded NEXRAD WSR-88D radar data. Computational and Information Systems Laboratory, NCAR, accessed 7 November 2019, https://doi.org/10.5065/D6NK3CR7.

Feng, Z., L. R. Leung, S. Hagos, R. A. Houze, C. D. Burleyson, and K. Balaguru, 2016: More frequent intense and long-lived storms dominate the springtime trend in central U.S. rainfall. *Nat. Commun.*, **7**, 13429, https://doi.org/10.1038/ncomms13429.

——, ——, R. A. Houze, S. Hagos, J. Hardin, Q. Yang, B. Han, and J. Fan, 2018: Structure and evolution of mesoscale convective systems: Sensitivity to cloud microphysics in convection-permitting simulations over the United States. *J. Adv. Model. Earth Syst.*, **10**, 1470–1494, https://doi.org/10.1029/2018MS001305.

——, R. A. Houze, R. Leung, F. Song, J. Hardin, J. Wang, W. I. Gustafson Jr., and C. R. Homeyer, 2019: Spatiotemporal characteristics and large-scale environments of mesoscale convective systems east of the Rocky Mountains. *J. Climate*, **32**, 7303–7328, https://doi.org/10.1175/JCLI-D-19-0137.1.

Ferguson, C. R., and E. F. Wood, 2011: Observed land–atmosphere coupling from satellite remote sensing and reanalysis. *J. Hydrometeor.*, **12**, 1221–1254, https://doi.org/10.1175/2011JHM1380.1.

Findell, K. L., and E. A. B. Eltahir, 2003a: Atmospheric controls on soil moisture–boundary layer interactions. Part I: Framework development. *J. Hydrometeor.*, **4**, 552–569, https://doi.org/10.1175/1525-7541(2003)004<0552:ACOSML>2.0.CO;2.

——, and ——, 2003b: Atmospheric controls on soil moisture–boundary layer interactions. Part II: Feedbacks within the continental United States. *J. Hydrometeor.*, **4**, 570–583, https://doi.org/10.1175/1525-7541(2003)004<0570:ACOSML>2.0.CO;2.

Ford, T. W., A. D. Rapp, S. M. Quiring, and J. Blake, 2015: Soil moisture–precipitation coupling: Observations from the Oklahoma Mesonet and underlying physical mechanisms. *Hydrol. Earth Syst. Sci.*, **19**, 3617–3631, https://doi.org/10.5194/hess-19-3617-2015.

——, S. M. Quiring, B. Thakur, R. Jogineedi, A. Houston, S. Yuan, A. Kalra, and N. Lock, 2018: Evaluating soil moisture–precipitation interactions using remote sensing: A sensitivity analysis. *J. Hydrometeor.*, **19**, 1237–1253, https://doi.org/10.1175/JHM-D-17-0243.1.

Fritsch, J. M., R. J. Kane, and C. R. Chelius, 1986: The contribution of mesoscale convective weather systems to the warm-season precipitation in the United States. *J. Climate Appl. Meteor.*, **25**, 1333–1345, https://doi.org/10.1175/1520-0450(1986)025<1333:TCOMCW>2.0.CO;2.

Froidevaux, P., L. Schlemmer, J. Schmidli, W. Langhans, and C. Schär, 2014: Influence of the background wind on the local soil moisture–precipitation feedback. *J. Atmos. Sci.*, **71**, 782–799, https://doi.org/10.1175/JAS-D-13-0180.1.

Frye, J. D., and T. L. Mote, 2010: Convection initiation along soil moisture boundaries in the southern Great Plains. *Mon. Wea. Rev.*, **130**, 1140–1151, https://doi.org/10.1175/2009MWR2865.1.

Guillod, B. P., and Coauthors, 2015: Reconciling spatial and temporal soil moisture effects on afternoon rainfall. *Nat. Commun.*, **6**, 6443, https://doi.org/10.1038/ncomms7443.

Haberlie, A. M., and W. S. Ashley, 2019: A radar-based climatology of mesoscale convective systems in the United States. *J. Climate*, **32**, 1591–1606, https://doi.org/10.1175/JCLI-D-18-0559.1.

Hersbach, H., and Coauthors, 2018: ERA5 hourly data on pressure levels from 1979 to present. Copernicus Climate Change Service (C3S) Climate Data Store (CDS), accessed 21 November 2019, https://doi.org10.24381/cds.bd0915c6.

——, and Coauthors, 2020: The ERA5 global reanalysis. *Quart. J. Roy. Meteor. Soc.*, **146**, 1999–2049, https://doi.org/10.1002/qj.3803.

Houze, R. A., Jr., 2004: Mesoscale convective systems. *Rev. Geophys.*, **42**, RG4003, https://doi.org/10.1029/2004RG000150.

——, 2018: 100 years of research on mesoscale convective systems. *A Century of Progress in Atmospheric and Related Sciences: Celebrating the American Meteorological Society Centennial, Meteor. Monogr.*, No. 59, Amer. Meteor. Soc., 17.11–17.54, https://doi.org/10.1175/AMSMONOGRAPHS-D-18-0001.1.

——, B. F. Smull, and P. Dodge, 1990: Mesoscale organization of springtime rainstorms in Oklahoma. *Mon. Wea. Rev.*, **118**, 613–654, https://doi.org/10.1175/1520-0493(1990)118<0613:MOOSRI>2.0.CO;2.

Janowiak, J. E., R. J. Joyce, and Y. Yarosh, 2001: A real-time global half-hourly pixel-resolution infrared dataset and its applications. *Bull. Amer. Meteor. Soc.*, **82**, 205–218, https://doi.org/10.1175/1520-0477(2001)082<0205:ARTGHH>2.3.CO;2.

Koster, R. D., 2004: Regions of strong coupling between soil moisture and precipitation. *Science*, **305**, 1138–1140, https://doi.org/10.1126/science.1100217.

Miralles, D. G., A. J. Teuling, C. C. van Heerwaarden, and J. V.-G. de Arellano, 2014: Mega-heatwave temperatures due to combined soil desiccation and atmospheric heat accumulation. *Nat. Geosci.*, **7**, 345–349, https://doi.org/10.1038/ngeo2141.

Muñoz Sabater, J., 2019: ERA5-land hourly data from 1981 to present. Copernicus Climate Change Service (C3S) Climate Data Store (CDS), https://doi.org/10.24381/cds.e2161bac.

Orbe, C., L. D. Oman, S. E. Strahan, D. W. Waugh, S. Pawson, L. L. Takacs, and A. M. Molod, 2017: Large-scale atmospheric transport in GEOS replay simulations. *J. Adv. Model. Earth Syst.*, **9**, 2545–2560, https://doi.org/10.1002/2017MS001053.

Parker, M. D., and R. H. Johnson, 2000: Organizational modes of midlatitude mesoscale convective systems. *Mon. Wea. Rev.*, **128**, 3413–3436, https://doi.org/10.1175/1520-0493(2001)129<3413:OMOMMC>2.0.CO;2.

Peters, J. M., and R. S. Schumacher, 2014: Objective categorization of heavy-rain-producing MCS synoptic types by rotated principal component analysis. *Mon. Wea. Rev.*, **142**, 1716–1737, https://doi.org/10.1175/MWR-D-13-00295.1.

Roundy, J. K., and J. A. Santanello, 2017: Utility of satellite remote sensing for land–atmosphere coupling and drought metrics. *J. Hydrometeor.*, **18**, 863–877, https://doi.org/10.1175/JHM-D-16-0171.1.

——, C. R. Ferguson, and E. F. Wood, 2014: Impact of land-atmospheric coupling in CFSv2 on drought prediction. *Climate Dyn.*, **43**, 421–434, https://doi.org/10.1007/s00382-013-1982-7.

Song, F., Z. Feng, L. R. Leung, R. A. Houze, J. Wang, J. Hardin, and C. R. Homeyer, 2019: Contrasting spring and summer large-scale environments associated with mesoscale convective systems over the U.S. Great Plains. *J. Climate*, **32**, 6749–6767, https://doi.org/10.1175/JCLI-D-18-0839.1.

Taylor, C. M., 2015: Detecting soil moisture impacts on convective initiation in Europe. *Geophys. Res. Lett.*, **42**, 4631–4638, https://doi.org/10.1002/2015GL064030.

——, and Coauthors, 2011: Frequency of Sahelian storm initiation enhanced over mesoscale soil-moisture patterns. *Nat. Geosci.*, **4**, 430–433, https://doi.org/10.1038/ngeo1173.

——, R. A. M. de Jeu, F. Guichard, P. P. Harris, and W. A. Dorigo, 2012: Afternoon rain more likely over drier soils. *Nature*, **489**, 423–426, https://doi.org/10.1038/nature11377.

Trier, S. B., C. A. Davis, and R. E. Carbone, 2014: Mechanisms governing the persistence and diurnal cycle of a heavy rainfall corridor. *J. Atmos. Sci.*, **71**, 4102–4126, https://doi.org/10.1175/JAS-D-14-0134.1.

Tuttle, J. D., and C. A. Davis, 2006: Corridors of warm season precipitation in the central United States. *Mon. Wea. Rev.*, **134**, 2297–2317, https://doi.org/10.1175/MWR3188.1.

Wang, S.-Y., T.-C. Chen, and E. S. Takle, 2011: Climatology of summer midtropospheric perturbations in the U.S. northern plains. Part II: Large-scale effects of the Rocky Mountains on genesis. *Climate Dyn.*, **36**, 1221–1237, https://doi.org/10.1007/s00382-010-0765-7.

Zhou, L., H. Chen, W. Hua, Y. Dai, and N. Wei, 2016: Mechanisms for stronger warming over drier ecoregions observed since 1979. *Climate Dyn.*, **47**, 2955–2974, https://doi.org/10.1007/s00382-016-3007-9.